Title
C-Terminal Turn Stability Determines Assembly Differences between Aβ40 and Aβ42

Journal
Journal of Molecular Biology, 425(2)

ISSN
0022-2836

Authors
Roychaudhuri, Robin
Yang, Mingfeng
Deshpande, Atul
et al.

Publication Date
2013

DOI
10.1016/j.jmb.2012.11.006

Peer reviewed

jmb Article

C-Terminal Turn Stability Determines Assembly Differences between Aβ40 and Aβ42

Robin Roychaudhuri[1†], Mingfeng Yang[1†], Atul Deshpande[2,3], Gregory M. Cole[2,3], Sally Frautschy[2,3], Aleksey Lomakin[4], George B. Benedek[4] and David B. Teplow[5]

*1 - **Department of Neurology,** David Geffen School of Medicine at UCLA, Los Angeles, CA 90095, USA*
*2 - **Department of Medicine,** UCLA, Los Angeles, CA 90095, USA*
*3 - **Greater Los Angeles Veterans Affairs Healthcare System,** Geriatric Research Education and Clinical Center, Sepulveda, CA 91343, USA*
*4 - **Center for Materials Science and Engineering and Department of Physics,** Massachusetts Institute of Technology, Cambridge, MA 02139, USA*
*5 - **Department of Neurology and Mary S. Easton Center for Alzheimer's Disease Research,** David Geffen School of Medicine, Molecular Biology Institute and Brain Research Institute, UCLA, Los Angeles, CA 90095, USA*

Correspondence to David B. Teplow: *dteplow@ucla.edu*
http://dx.doi.org/10.1016/j.jmb.2012.11.006
Edited by S. Radford

Abstract

Oligomerization of the amyloid β-protein (Aβ) is a seminal event in Alzheimer's disease. Aβ42, which is only two amino acids longer than Aβ40, is particularly pathogenic. Why this is so has not been elucidated fully. We report here results of computational and experimental studies revealing a C-terminal turn at Val36–Gly37 in Aβ42 that is not present in Aβ40. The dihedral angles of residues 36 and 37 in an Ile31–Ala42 peptide were consistent with β-turns, and a β-hairpin-like structure was indeed observed that was stabilized by hydrogen bonds and by hydrophobic interactions between residues 31–35 and residues 38–42. In contrast, Aβ(31–40) mainly existed as a statistical coil. To study the system experimentally, we chemically synthesized Aβ peptides containing amino acid substitutions designed to stabilize or destabilize the hairpin. The triple substitution Gly33Val–Val36Pro–Gly38Val ("VPV") facilitated Aβ42 hexamer and nonamer formation, while inhibiting formation of classical amyloid-type fibrils. These assemblies were as toxic as were assemblies from wild-type Aβ42. When substituted into Aβ40, the VPV substitution caused the peptide to oligomerize similarly to Aβ42. The modified Aβ40 was significantly more toxic than Aβ40. The double substitution D-Pro36–L-Pro37 abolished hexamer and dodecamer formation by Aβ42 and produced an oligomer size distribution similar to that of Aβ40. Our data suggest that the Val36–Gly37 turn could be the *sine qua non* of Aβ42. If true, this structure would be an exceptionally important therapeutic target.

Introduction

Alzheimer's disease (AD) is the most common cause of late-life dementia.[1] The predominant cerebral neuropathological features of AD are extracellular amyloid deposits formed by the amyloid β-protein (Aβ), intracellular neurofibrillary tangles formed by the protein tau, and neuron loss.[2] Aβ is a product of proteolytic cleavage of the Aβ precursor (AβPP).[3] Two predominant species of Aβ exist in humans, Aβ40 and Aβ42, which are distinguished by the absence or presence, respectively, of an Ile–Ala dipeptide at the C-terminal end of an identical 40-amino-acid peptide.[4] Aβ42 is the principal protein component of parenchymal plaques.[5–7] An increase in the absolute amount of Aβ42, or in the Aβ42/Aβ40 concentration ratio, is associated with familial forms of AD.[8,9] In humans, reduction of Aβ42 concentration correlates with a decreased risk for AD.[10] *In vitro* studies have shown that Aβ42 displays fibril nucleation and elongation rates that are significantly higher than

those of Aβ40[11] and that Aβ42 forms larger oligomers than does Aβ40.[12–16] Importantly, the assemblies formed by Aβ42 are more toxic than are those formed by Aβ40.[17]

To execute strategies for knowledge-based design of therapeutic agents, one must move from the regimes of morphology and kinetics to that of atomic structure and dynamics. In this way, specific atoms and their movements can be correlated with the biological consequences of peptide folding and assembly, providing critical information for drug targeting and design. Previously, we used the method of photo-induced cross-linking of unmodified proteins (PICUP) to determine quantitatively the oligomer size frequency distribution.[15,18] Aβ40 and Aβ42 oligomerized through distinct pathways. Aβ40 predominately assembled into dimeric, trimeric, and tetrameric species, whereas Aβ42 formed pentamer/hexamer units (paranuclei) that further assembled into larger oligomers (dodecamers, octadecamers).[19] These results were confirmed and extended using ion mobility spectrometry–mass spectrometry.[14] Other dodecameric structures also have been described, including Aβ-derived diffusible ligands[20] and Aβ*56.[21] In addition, many other types of assemblies, ranging in size from dimer to micrometer-sized macrostructures (βamy balls[22]), have been reported (for a recent review, see Roychaudhuri *et al.*[3]).

To elucidate, at atomic resolution, the conformational dynamics of Aβ40 and Aβ42 that contribute to their distinct physical and biological behaviors, we previously performed simulations on the respective monomeric Aβ peptides.[23] Initial studies using discrete molecular dynamics simulations with a four-bead peptide model showed that the C-terminal region was more structured in Aβ42 than in Aβ40 and was the key region driving Aβ42 assembly, whereas the central hydrophobic cluster dominated Aβ40 assembly.[24] In a later study, we observed that both peptides were largely disordered but that frequent turn-like features were exhibited by residues 6–9 (Turn #1, "T1"), 14–16 (T2), and 23–27 (T3). All three regions exist in both Aβ40 and Aβ42; thus, it is reasonable to speculate that these regions cannot alone contribute significantly to the idiotypic behavior of Aβ42. However, we did observe distinct behavior of the Aβ42 C-terminus (residues 31–42). This peptide segment tended to bend, resulting in the formation of a turn-like fold, involving residues 35–38 (T4), with a significantly larger number of intramolecular contacts than observed in Aβ40. Computational and experimental studies have shown that both peptides display little regular structure, but that the Aβ42 C-terminus is more rigid than that of Aβ40.[25–27] Lazo *et al.* showed that the Aβ42 C-terminus is resistant to proteolytic digestion.[28] Taken together, these data suggest the existence of a folded structure at the Aβ42 C-terminus.

We discuss here the results of computational and experimental studies seeking to test the hypothesis that the C-terminal turn[‡] element is the *sine qua non* of Aβ42, the structural feature that imparts on Aβ42 its unique assembly properties and biological activity relative to Aβ40.

Results

Simulation of Aβ C-terminal conformational dynamics

We used replica-exchange molecular dynamics (REMD) simulations for a total of 3.2 μs to generate 20,000 conformations for Aβ(31–40/42). To determine whether the simulation had converged, we divided the conformational ensemble into two equal parts. Each part was subjected to secondary-structure analysis using the DSSP program.[29] The highly overlapped curves shown in (Fig. 1) suggest that the two conformational ensembles are similar, which in turn indicates convergence of the simulations. Demonstrating convergence was important because it showed that our simulation sampled sufficient volumes of the total conformational space to produce a representative subset of that space, from which meaningful data could be obtained.

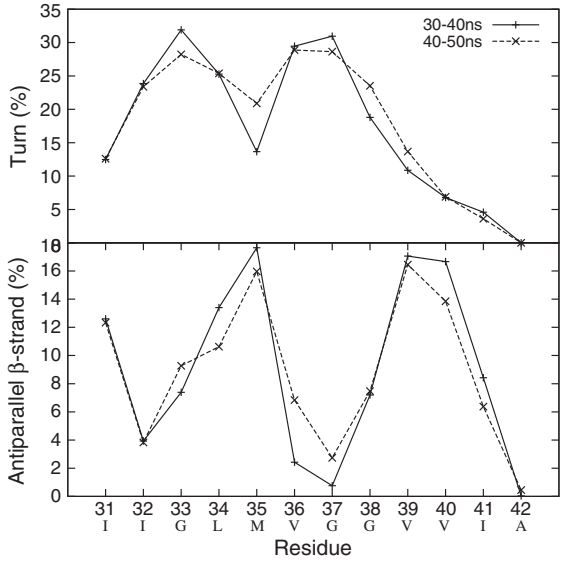

Fig. 1. The conformational ensemble collected from the REMD simulation of Aβ42 was divided into two equal populations of 10,000 conformers each. Each population was then subjected to secondary-structure analysis using the DSSP program[29] to determine the percentages of turn (upper panel) and antiparallel β-sheet (lower panel). The highly overlapped curves suggest that the two conformational ensembles are similar, indicating convergence of the simulations.

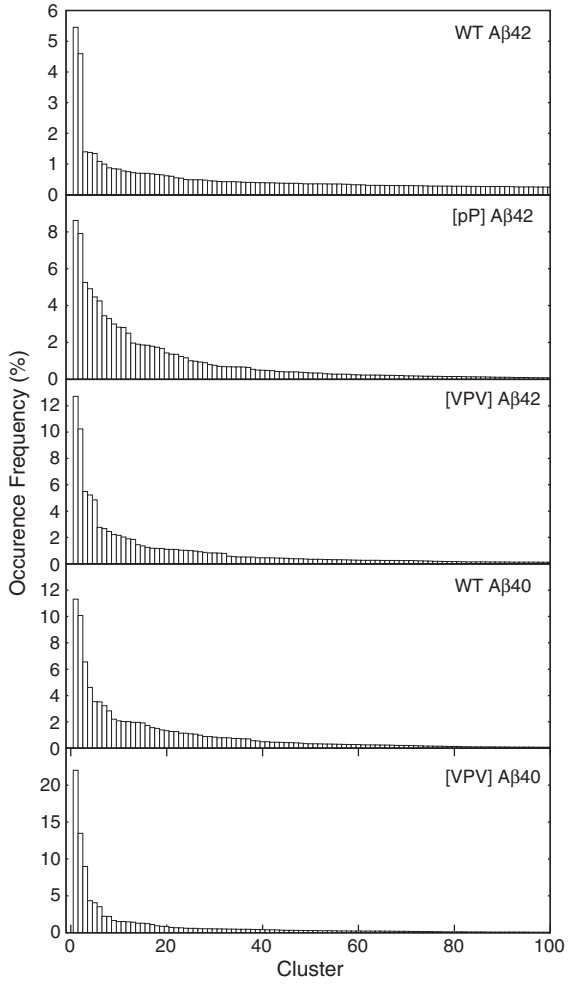

Fig. 2. Occurrence frequencies (%) for each conformational cluster of each Aβ peptide.

We then clustered the collected conformations with an RMSD threshold of 2 Å (Fig. 2). Though the Aβ42 C-terminus appears to be disordered overall, its most populated structure is a well-folded β-hairpin with residues 36 and 37 located at the $i+1$ and $i+2$ positions of the β-turn (Fig. 3, red arrows). This β-hairpin structure is stabilized by hydrogen bond interactions between Ile31:Ala42, Ile32:Ile41, Gly33:Val40, Leu34:Val39, and Met35:Gly38 and hydrophobic interactions between Ile31:Ile41, Leu34:Val39, and Val40:Met35. The second most populated C-terminus structure is also compact and contains a well-defined β-turn at residues 35–38 (Fig. 4). The occurrence frequency for these two structures combined is ≈10 times greater than the third most populated structure (Fig. 2). For this reason, we do not discuss the third most frequent conformational clusters or clusters of even smaller occurrence frequency. We also calculated the dihedral angles of residues 36 and 37 to quantify β-turn content, as the propensity of residues 36 and 37 to exist in a β-turn is closely related to the stability of the β-hairpin. The turn type adopted by residues 36 and 37 is not unique, as type I′, type II, and βVIb turns were observed at frequencies of 10%, 7.5%, and 7%, respectively (Table 1). We refer to these turns collectively as "β-turns." In contrast to these data from Aβ42, the most populated Aβ40 C-terminus conformer displayed no regular secondary structure, and β-turn population by residues 35–38 (8%) was $<1/3$ that of Aβ42 (Table 1).

Conformational dynamics of designed C-terminal peptide analogues

If the β-hairpin structure determined were a relevant structural feature of holo-Aβ, we hypothesized that it should be possible to design *de novo* Aβ analogues containing amino acid substitutions that would stabilize the β-hairpin. To test this hypothesis, we first used MD simulations to determine whether specific amino acids would indeed stabilize the β-hairpin (Table 1). The first Aβ(31–42) peptide we designed contained D-Pro36–L-Pro37, as this sequence has been shown to stabilize β-hairpin structure significantly.[30] This peptide is designated [*pP*]Aβ42. Unexpectedly, the simulation revealed that though significantly more (50%) β-turn structure was observed for residues 35–38, the most populated structure was actually a statistical coil (SC) and the overall conformational diversity was higher than that of wild-type Aβ(31–42) (Figs. 2 and 3). This peptide thus was studied to determine how destabilizing substitutions affected peptide dynamics.

We then designed a second Aβ42 analogue, but with an L-Pro36–L-Gly37 sequence that was reported to stabilize β-hairpin structure.[31,32] In this peptide, we also replaced Gly33 and Gly38 with Val to reduce the flexibility of the peptide backbone and to strengthen putative hydrophobic interactions between the two predicted β-strands. We designate this peptide [*VPV*]Aβ42. With these modifications, β-hairpin content increased from 5.5% to 12.5%, and the β-turn population increased to 65%, as revealed by MD simulation (Figs. 2 and 3).

Because the [*pP*] substitution in Aβ42 did not stabilize its turn, we did not incorporate it into Aβ40 (see Fig. 3 for wild-type Aβ40 conformers). Instead, we focused on [*VPV*]Aβ40. We observed that this substitution did not produce a β-hairpin structure (Figs. 2 and 3), though higher β-turn content (35%) was observed for residues 35–38 (Table 1).

Peptide secondary-structure dynamics

To determine the temporal dynamics of peptide secondary structure, we monitored peptide assembly using CD (Figs. 5 and 6). Wild-type Aβ42 and Aβ40 initially displayed SC structures (Fig. 5a and b, respectively), which underwent rapid SC→β-sheet transitions to produce maximal β-sheet levels of

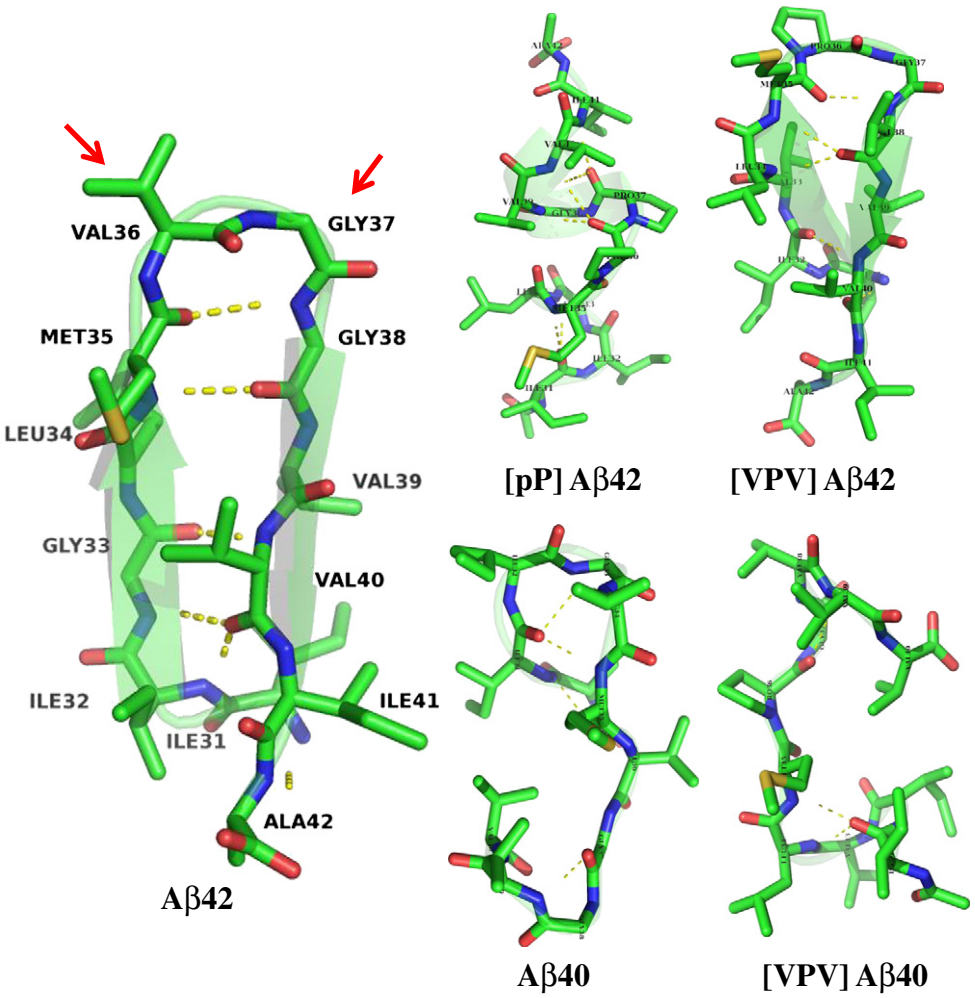

Fig. 3. Structures of the most populated conformers for each peptide. Yellow dotted lines indicate hydrogen bonds. C, N, O, and S atoms are colored green, blue, red, and yellow, respectively. H atoms are not shown. Red arrows point toward the turn, residues 36 and 37. Each of the five conformers overlays a ribbon diagram of its own peptide backbone to help illustrate the position of the backbone and any secondary-structure elements within it.

≈40–45% by days 4 and 5, respectively (Fig. 6). Relative to Aβ42, and to all the other peptides, [*VPV*] Aβ42 displayed significantly more β-structure initially (≈30%) and showed maximal β-structure at day 5 (Figs. 5 and 6). [*VPV*]Aβ40 displayed slower kinetics, not displaying maximal β-sheet structure until day 8 (Figs. 5d and 6). In contrast to the structural transitions observed for the other peptides, [*pP*]Aβ42 remained as an SC throughout the experiment (Figs. 5e and 6).

Time evolution of β-sheet structure

Thioflavin T (ThT) fluorescence was used to monitor the time dependence of β-sheet formation during Aβ incubation (Fig. 7).[34] Aβ40 and Aβ42 displayed rapid rises in fluorescence that peaked at days 4 and ≈2, respectively. These peaks were followed by declines, an observation that is typical for Aβ assembly.[35] We did not observe a lag phase because relatively high peptide concentrations were used (≈35–40 μM). [*VPV*]Aβ40 displayed a monotonic increase in fluorescence that started at day 1 and peaked at day 6 at a level somewhat higher than that produced by Aβ40. [*VPV*]Aβ42, in contrast, produced substantial fluorescence immediately. The fluorescence intensity was ≈40% that of the maximal level displayed by Aβ42. The fluorescence remained relatively constant, or trended slightly downward, during the observation period. [*pP*]Aβ42 showed a very modest monotonic increase in fluorescence over time, producing a final fluorescence intensity that was <5% of the maximum levels of Aβ40 or Aβ42.

Peptide oligomerization

To determine the effects of the designed amino acid substitutions on peptide oligomerization, we

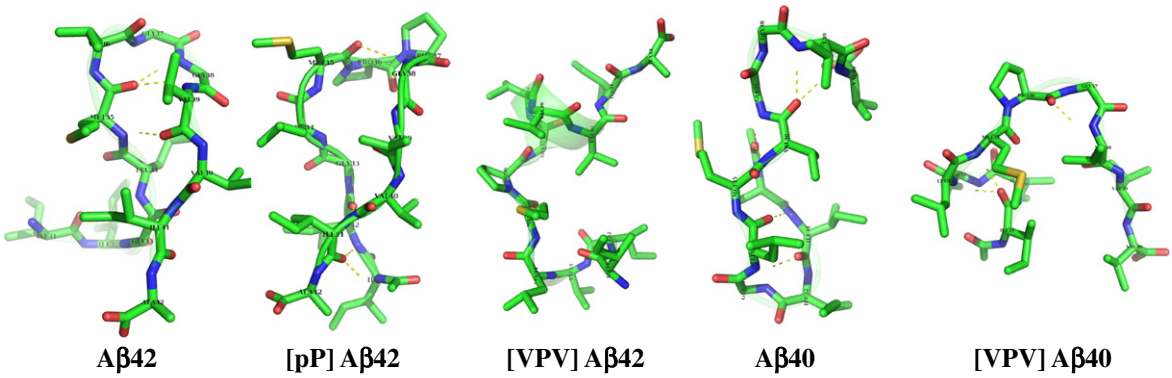

Fig. 4. Structures of the second most populated conformers for each peptide. Yellow dotted lines indicate hydrogen bonds. C, N, O, and S atoms are colored green, blue, red, and yellow, respectively. H atoms are not shown. Each of the five conformers overlays a ribbon diagram of its own peptide backbone to help illustrate the position of the backbone and any secondary-structure elements within it.

used the technique of PICUP.[36] PICUP enables quantitative determination of the oligomer size frequency distribution. Cross-linking Aβ40 and Aβ42 produced typical distributions;[15] namely, Aβ40 formed oligomers predominately of orders[§] 2–4 (Fig. 8, lane 5) and Aβ42 formed oligomers of orders 2–6 (Fig. 8, lane 3). Un-cross-linked Aβ40 displayed only a monomer band, whereas un-cross-linked Aβ42 displayed monomer and trimer bands (results not shown), as has been reported previously.[15] The [*VPV*]Aβ42 peptide oligomerized distinctly from its wild-type homologue (Fig. 8, lane 2). Prominent bands were observed with molecular masses of ≈4.5 kDa, ≈23 kDa, and ≈28 kDa, corresponding to monomer, pentamer, and hexamer, respectively. Relatively faint bands with molecular masses of ≈9 kDa and ≈18 kDa, corresponding to dimer and tetramer, were observed. No trimer band was observed. Bands of molecular mass ≈42–56 kDa also were seen. These bands may correspond to nonamer–dodecamer. In contrast, the oligomer distribution of [*pP*]Aβ42 (Fig. 8, lane 1) was very similar to that of Aβ40, with the exception that the apparent molecular masses of each band were slightly higher due to the increased mass of this substituted Aβ42 peptide. The oligomer distribution of [*VPV*]Aβ40 (Fig. 8, lane 4) was distinct from that of wild-type Aβ40 (Fig. 8, lane 5). The [*VPV*]Aβ40 distribution was characterized by four prominent bands, monomer, dimer, a band between trimer and tetramer, and a band between tetramer and pentamer. This distribution displayed similarities to the distribution of wild-type Aβ42 in its relative paucity of trimer and greater abundance of higher-order oligomers.

Temporal changes in peptide assembly size

Dynamic light scattering (DLS) was used to monitor time-dependent changes in the distribution of oligomer sizes (Fig. S1). No significant time-dependent changes in the oligomer distributions of Aβ40 or [*VPV*]Aβ40 peptides were observed over a time period of 1 month. Both peptides formed small oligomers (R_H ≈ 2 nm) and a broad distribution of larger assemblies. In Aβ40, assemblies of R_H ≈ 10 nm and large aggregates with R_H ≈ 60–80 nm were observed. In addition, occasional contributions to the scattering intensity from very large (many hundreds of nanometers) were observed. These contributions increased over time, as reflected by the decreasing scattering intensity noted for the shaded oligomer peaks. Additionally, numerous intensity spikes appeared after a few days (data not shown). Such intensity spikes indicate formation of very large aggregates that drift in and out of the scattering volume.

Table 1. Amino acid substitutions engineered into the Aβ sequence

Aβ	Sequence	Structure[a]	β-Turn[b] (%)	Oligomers formed[c]
Aβ42	^{31}IIGLMVGGVVIA	β-Hairpin	25	1, 2, 3, 4, 5, 6
[*VPV*]Aβ42	^{31}II***V***LM***P***G***V***VIA	β-Hairpin	65	1, 5, 6, 12
[*pP*]Aβ42	^{31}IIGLM***pP***GVVIA	Statistical coil	50	1, 2, 3, 4
Aβ40	^{31}IIGLMVGGVV	Statistical coil	8	1, 2, 3, 4
[*VPV*]Aβ40	^{31}II***V***LM***P***G***V***VV	Statistical coil	35	1, 3, 5

The substituted positions are highlighted in bold italics. Lowercase p signifies D-Pro.
[a] Structure of the predominant full-length conformer in the population.
[b] Structure of residues 35–38 defined by dihedral angle.
[c] Numbers indicate the assembly "order," that is, the number of monomers per oligomer, observed by SDS-PAGE. Monomers are signified by "1."

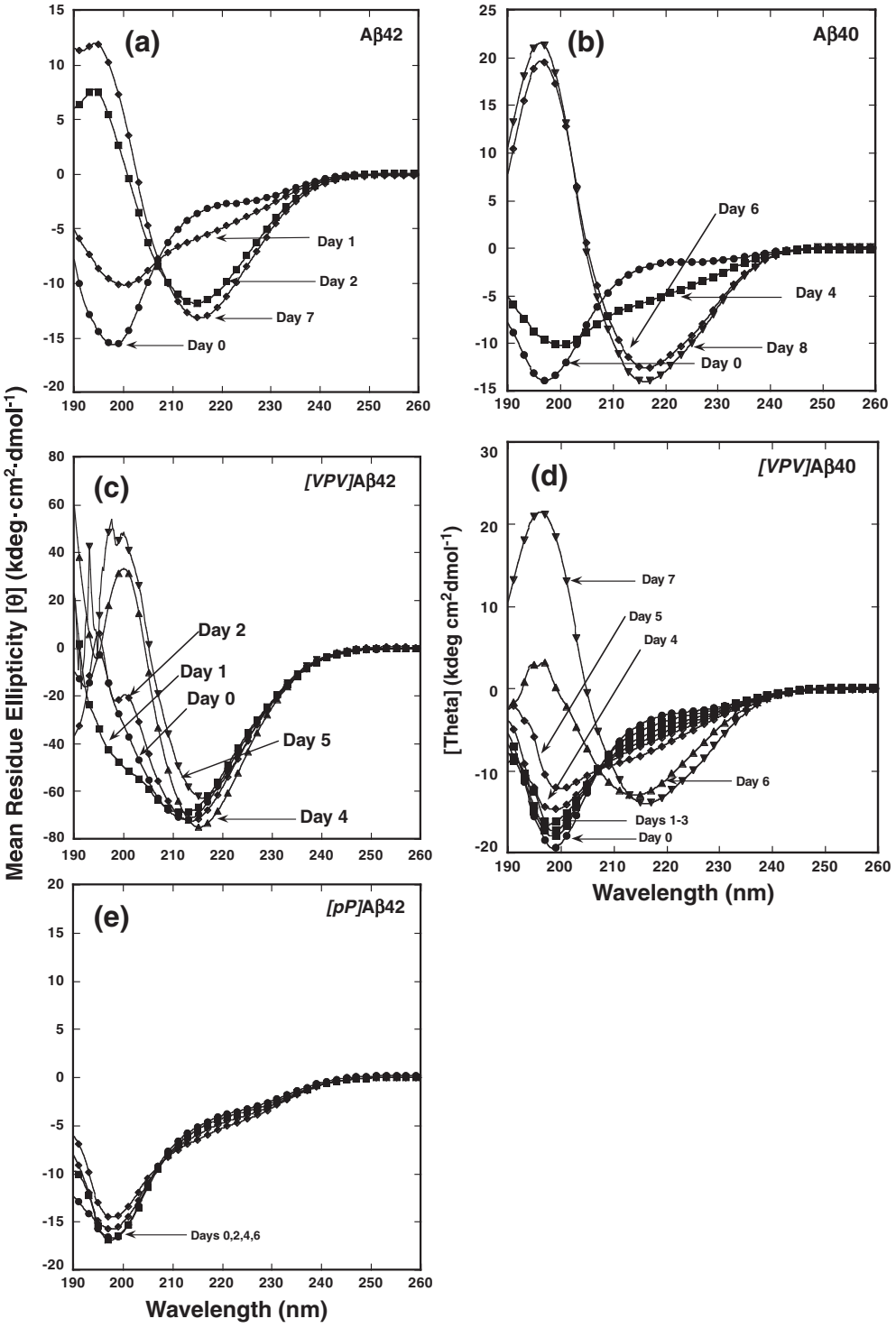

Fig. 5. CD spectroscopy. LMW Aβ solutions were prepared at concentrations of 60–80 μM and then incubated at 37 °C with slow inversion. Aliquots were removed periodically for CD analysis. (a) Aβ42, (b) Aβ40, (c) [*VPV*]Aβ42, (d) [*VPV*]Aβ40, (e) [*pP*]Aβ42. The spectra are representative of those obtained in each of three independent experiments. Spectra from different days that were essentially superimposable are represented by a single spectrum, for clarity of viewing.

In comparison to the Aβ40 system, Aβ42 and [*VPV*]Aβ42 displayed more prominent contributions from oligomers. This means that many fewer 60- to 80-nm aggregates were present. The oligomer fraction remained stable over a month of observation. In addition, oligomers of [*VPV*]Aβ42 had

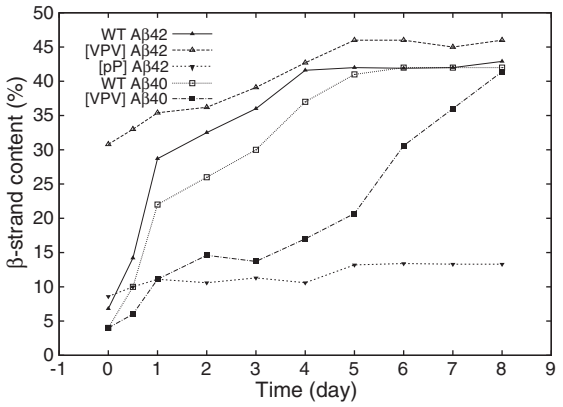

Fig. 6. Kinetics of β-strand formation. Data from the experiments shown in Fig. 5 were deconvolved using DichroWeb[33] to yield percent β-strand content for each peptide on each day of observation. These data then were combined to produce the figure shown.

$R_H \approx 8$ nm. This size was less than the 10-nm size typically observed in Aβ42 experiments[19,37] and may reflect a difference in oligomer structure of Aβ42 and [*VPV*]Aβ42. Interestingly, [*pP*]Aβ42 behaved much more like Aβ40. It predominantly formed small oligomers with $R_H \approx 2$ nm, and no significant increase in size occurred. Some larger aggregates were present that had $R_H \approx 20$–30 nm. These aggregates were much smaller than those in the Aβ40 samples and scattered much less light. As a consequence, the relative contribution of the 2-nm oligomer fraction in [*pP*]Aβ42 was very prominent.

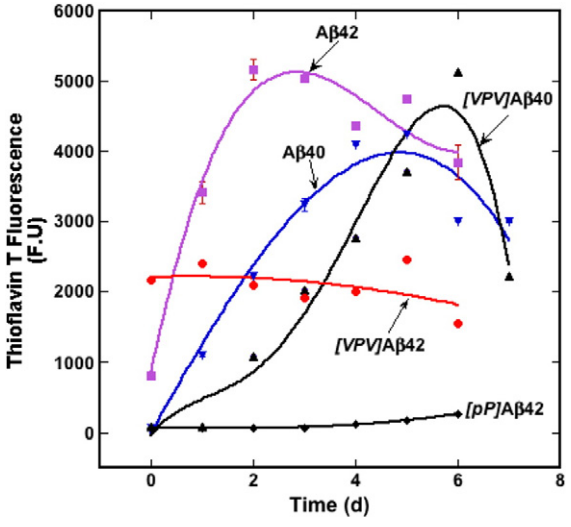

Fig. 7. Kinetics of β-sheet formation. Peptides were incubated in 10 mM phosphate buffer, pH 7.4, for 7 days at 37 °C with slow inversion. Aliquots were removed every 24 h to determine the level of ThT fluorescence. Error bars show standard error, which, in some cases, are smaller than the figure symbols.

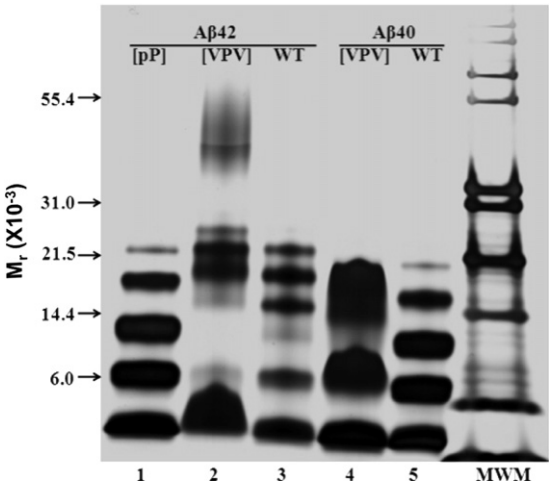

Fig. 8. Analysis of Aβ oligomerization. Each peptide was solvated freshly from the lyophilized state and then immediately subjected to PICUP, followed by SDS-PAGE and silver staining. Lane 1, [*pP*]Aβ42; lane 2, [*VPV*]Aβ42; lane 3, Aβ42; lane 4, [*VPV*]Aβ40; and lane 5, Aβ40. "MWM" is molecular weight marker. The data in the experiment shown are essentially identical with those observed in two other independent experiments performed on different days.

Aβ assembly morphology

To determine if assembly stage-specific differences in morphology existed among the different Aβ peptides, we examined aliquots of the assembly reactions using electron microscopy (EM). The kinetics of assembly differs among the peptides. For this reason, examination of different peptide samples at the same times would not allow morphologic comparisons of each peptide at the same stage of assembly. To control for this variance, we used a temporal normalization procedure. In an independent set of experiments, we monitored the time-dependent evolution of β-sheet structure. We determined β-sheet content at the initiation of peptide incubation ($t_\beta = 0\%$) and at the time at which β-sheet content was maximal ($t_\beta = 100\%$). We then determined the half-time ($t_\beta = 50\%$) for this process. Within experimental error, this kinetics was reproducible, which allowed us in subsequent experiments to remove aliquots of each peptide for EM analysis at equivalent assembly stages. However, in addition, CD monitoring was done on the actual samples used for EM to ensure that aliquot removal was done at equivalent stages. Each aliquot was frozen in liquid nitrogen and stored at −80 °C until analysis. Importantly, the thawed samples were used concurrently for EM and cytotoxicity assays (see below) to ensure that rigorous structure–activity correlations could be accomplished.

Initially, small (10–30 nm diameter) circular or irregular structures were observed in the Aβ40

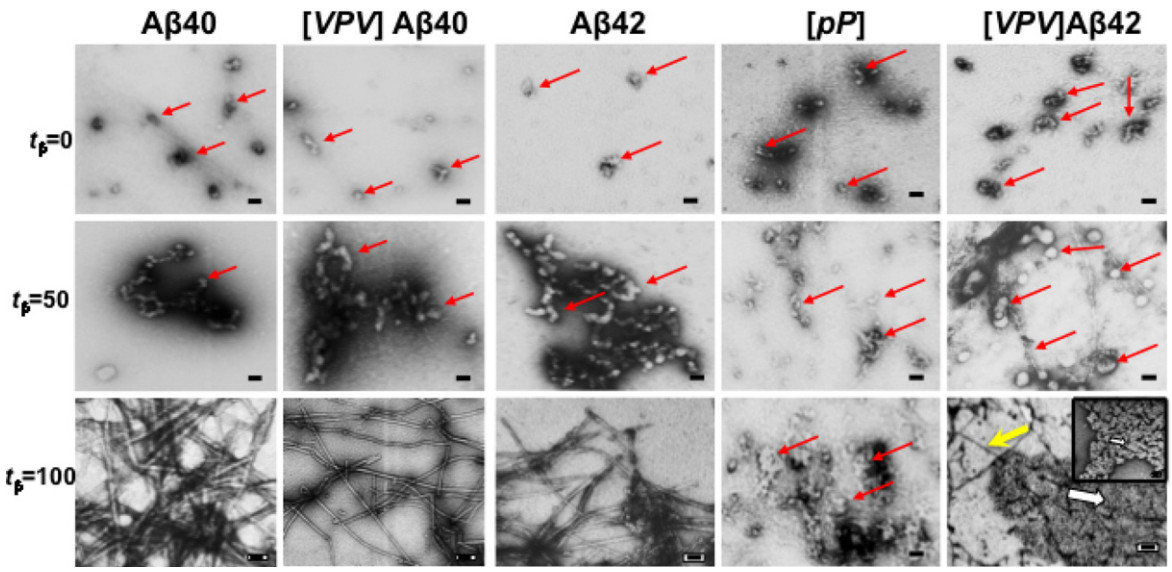

Fig. 9. Morphology of peptide assemblies. Electron micrographs of Aβ40, Aβ42, and their analogues at $t_β$ = 0%, 50%, and 100% (0%, 50%, and 100% points in the process of β-sheet formation: see the text for explanation). Red arrows point to structures discussed in the text. In the plate of [*VPV*]Aβ42 at $t_β$ = 100, a yellow arrow shows a thin filament and a thick white arrow points to the section of the micrograph expanded in the inset, in which a smaller white arrow points to a railroad-track-like structure. Magnification is 29,000×. The scale bar represents 100 nm.

(Fig. 9, panel $t_β$ = 0) and Aβ42 (Fig. 9, panel $t_β$ = 0) samples. [*VPV*]Aβ40 formed structures that were larger than those of Aβ40, ≈20–30 nm in diameter compared with ≈10–20 nm. Each of the [*VPV*]Aβ mutants produced structures that were larger in size than their wild-type Aβ42 counterparts and often were found clumped into larger superstructures. [*VPV*]Aβ42 formed a mixture of spherical oligomers ranging in size from 13 to 20 nm and worm-like aggregates that were ≥100 nm in size. [*pP*]Aβ42 formed comparatively smaller structures than did [*VPV*]Aβ42.

At $t_β$ = 50% point in assembly, Aβ40 and [*VPV*]Aβ40 formed aggregates containing globular units of 5–10 nm diameter and 10–40 nm diameter, respectively. Aβ42 formed globular species with diameter ranging from 20 to 30 nm. [*VPV*]Aβ42 formed globular structures ranging in diameter from 50 to 100 nm. Small numbers of fibrils, with diameters of 10–20 nm, also were observed. [*pP*]Aβ42 formed comparatively smaller structures than did [*VPV*]Aβ42. Some irregular structures had diameters of 20 nm. Others appeared to cluster in aggregates with sizes ranging from 40 to 100 nm. Each respective Aβ assembly formed at $t_β$ = 50% was larger than that observed at $t_β$ = 0%.

Cursory examination of the [*VPV*]Aβ42 assemblies suggested that the distribution of sizes might not be continuous. For this reason, we determined quantitatively the size frequency distribution of the assemblies (Fig. 10). The distribution showed that the predominant assembly diameter was 50 nm. Substantial numbers of structures with diameters of 36 nm, 43 nm, and 57 nm also were observed. At $t_β$ = 100%, Aβ40 and [*VPV*]Aβ40 formed fibrils that ranged in diameter from 5 to 10 nm and from 8 to 10 nm, respectively. Aβ42 produced a dense meshwork of fibrils with diameters of 10–15 nm. Many of the fibrils appeared helical with a pitch of ≈40 nm. [*VPV*]Aβ42 displayed quasicrystalline structures (Fig. 9, white arrow), along with fibrils. The quasicrystalline structures were 20–60 nm in length and 40–80 nm in diameter and resembled railroad tracks and ties (Fig. 9, inset). Needle-like fibrils also were observed (Fig. 9, yellow arrow), and these had diameters of 5 nm, thinner than those of Aβ42. In contrast to the other four peptides, [*pP*]Aβ42 did not form fibrils but rather remained in a relatively amorphous state characterized by masses of assemblies dispersed throughout the grid.

Cytotoxicity assays

To establish structure–activity relationships, we performed two types of cytotoxicity assays, MTS (3-[4,5-dimethylthiazol-2-yl]-5-[3-carboxymethoxyphenyl]-2-[4-sulfophenyl]-2*H*-tetrazolium) and LDH (lactate dehydrogenase). The MTS assay was employed to evaluate the effects of the assemblies on cellular metabolism, including MTS reduction and exocytosis, and the LDH assay was performed to evaluate cell viability (plasma membrane integrity).[38] Aβ samples were prepared as they were for EM studies and then the samples were added to rat primary hippocampal and cortical neurons.

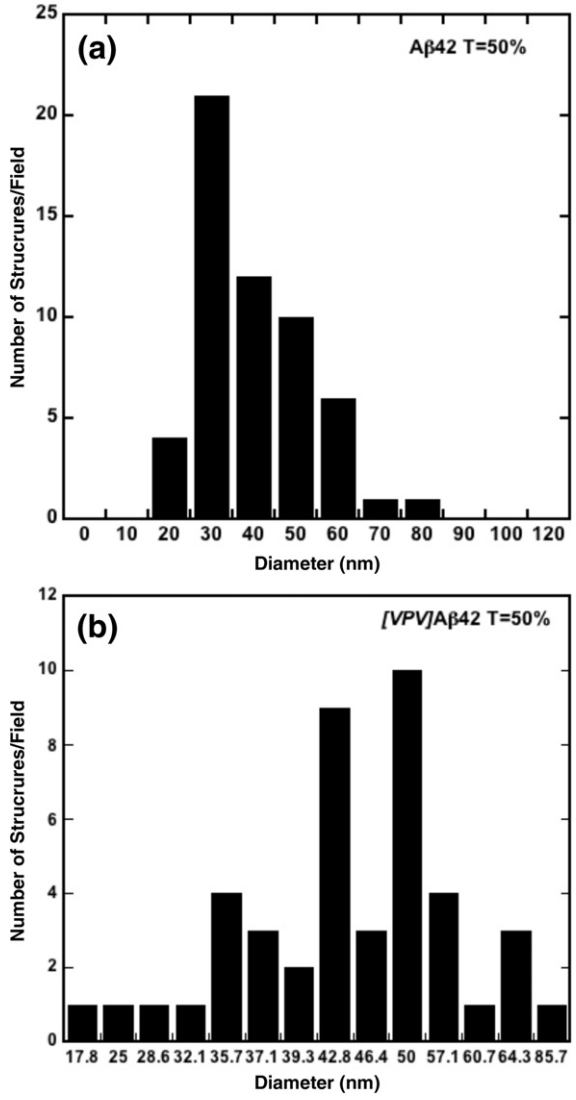

Fig. 10. Histograms of assembly diameters observed by EM of Aβ42 (a) and [*VPV*]Aβ42 (b) at $t_\beta = 50\%$. The total number of structures examined was 56 and 44, respectively.

Samples assayed immediately after preparation ($t_\beta = 0\%$) had no significant effect on MTS metabolism (Fig. 11). However, at $t_\beta = 50\%$, all the peptides except Aβ40 were toxic ($p < 0.01$). The toxicity of [*VPV*]Aβ40 trended lower than those of the Aβ42 peptides, but this difference was not statistically significant. At $t_\beta = 100\%$, [*pP*]Aβ42, [*VPV*]Aβ42, and [*VPV*]Aβ40 remained as toxic as they were at $t_\beta = 50\%$. The toxicity of Aβ42 trended toward greater toxicity than the control, but the difference was insignificant statistically. Aβ40 remained nontoxic.

Results for the LDH assay were consistent with those of the MTS assay (Fig. 12). At $t_\beta = 0\%$, no significant toxicity was observed for any of the peptides. At $t_\beta = 50\%$, large, statistically significant ($p < 0.01$) increases in LDH activity were seen for all

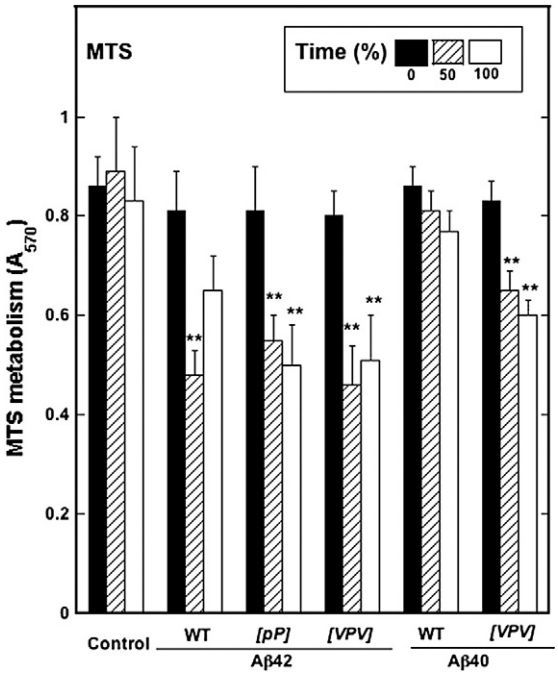

Fig. 11. MTS activity as measured in rat primary hippocampal and cortical neurons for the different Aβ peptides and their substitutions at $t_\beta = 0\%$, 50%, and 100%. Absorbance was measured at 570 nm.

the Aβ42 peptides and for [*VPV*]Aβ40. Aβ40 toxicity was significantly higher than that of the control ($p < 0.05$), but the absolute increase was small. The

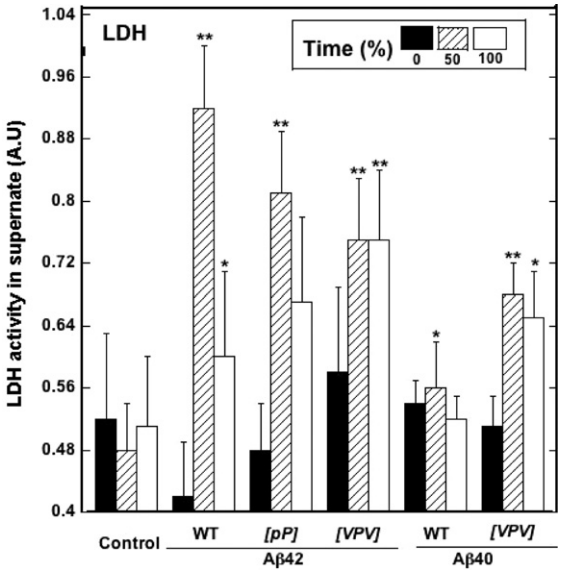

Fig. 12. LDH toxicity assays of Aβ assemblies. Aliquots removed from the samples used for CD experiments were used to treat rat primary hippocampal and cortical neurons. LDH activity released into the medium was used to assess assembly toxicity. $^{**}p < 0.01$ compared to control and $^{*}p < 0.05$ compared to control. Error bars are ±SD.

absolute toxicity levels of the Aβ42 assemblies were higher than those of the Aβ40 assemblies. At t_β = 100%, Aβ42 peptide toxicities remained approximately equal to, or were lower than, those observed for the same peptides at t_β = 50%. However, in all cases, significant ($p < 0.01$) toxicity was observed (*versus* controls). Aβ40 was not toxic at t_β = 100%, whereas the toxicity of [*VPV*]Aβ40 remained identical, within experimental error, to that observed at t_β = 50%.

Discussion

Aβ40 and Aβ42 have been found to oligomerize in two distinct manners. Aβ40 forms primarily dimers, trimers, and tetramers, whereas Aβ42 assembles into pentamer/hexamer units (paranuclei) that can self-associate to produce dodecamers and hexadecamers.[14,19] Interestingly, experimental and *in silico* studies suggest that the overall conformational dynamics of the two peptides are similar, with the exception of their C-termini.[25–27] The C-terminus of Aβ42 is more rigid, an observation likely due to the more frequent intramolecular contacts within this segment.[23] In this study, we first used REMD simulations to extensively sample and then compare the conformational spaces of Aβ(31–42) and Aβ(31–40) foldons. We discovered that the most populated conformational cluster of Aβ(31–42) was a β-hairpin-like structure with a β-turn centered at V36–G37, whereas Aβ(31–40) existed predominately as an SC (Figs. 2 and 3).

We hypothesized that if this β-hairpin conformation was the key structural element responsible for the distinct oligomerization behavior of Aβ40 and Aβ42, then we could perturb oligomerization by engineering stabilizing or destabilizing amino acid substitutions in this region, a study that would have important implications for targeting therapeutic agents. To test our hypothesis, we first engineered [*pP*]Aβ42, in which V36 and G37 were replaced by D-Pro and L-Pro, respectively. The D-Pro–L-Pro dipeptide is known to effectively constrain the backbone dihedral angles in a region favoring β-turn structure.[30] Surprisingly, simulations using [*pP*]Aβ(31–42) revealed that this peptide segment mostly existed as SC. We interpret this result as an effect of the positive entropic contribution of the two Gly residues at 33 and 38, which favors a flexible conformer.

We next engineered [*VPV*]Aβ42, in which G33, V36, and G38 were replaced by Val, L-Pro, and Val, respectively. The G33→V and G38→V replacements should increase the rigidity of the backbone, as well as the hydrophobic interaction between the two β-strands. The L-Pro–Gly sequence is known to constrain the β-turn conformation. As predicted, the β-hairpin population of [*VPV*]Aβ(31–42) nearly doubled compared with Aβ(31–42) (Fig. 2). The increased stability of β-hairpin was reflected by the fact that [*VPV*]Aβ42 displayed high β-content immediately after dissolution, whereas Aβ42 existed in SC form after 5 days of incubation. ThT fluorescence results were consistent with these observations. Wild-type Aβ40 and Aβ42 exhibited progressive increases in ThT binding as fibril formation proceeded. In contrast, [*VPV*]Aβ42 produced substantial ThT fluorescence immediately upon solvation, and the fluorescence intensity remained nearly constant during the duration of the experiment. These results suggest that substantial and increased β-sheet formation, relative to that found in wild-type Aβ42, occurs in [*VPV*]Aβ42 and that this β-sheet structure is stable. Fourier transform infrared experiments have suggested that antiparallel β-sheet is a structural signature of Aβ42 oligomers,[39] and this feature is consistent with our model of the Aβ42 C-terminus as a β-hairpin. DLS experiments also revealed that [*VPV*]Aβ42 formed oligomers that were more stable than those of Aβ42 (Fig. S1).

To investigate how the stabilized and destabilized β-turn affected oligomerization, we used PICUP and SDS-PAGE (Fig. 8). Stabilization of the β-turn, in the form of the [*VPV*]Aβ42 peptide, produced a tri-nodal distribution involving primarily monomer, pentamer/hexamer, and nonamer. The decreased dispersity of this distribution combined with the appearance of higher-order oligomers is consistent with the behavior of a peptide that could be characterized as a "super Aβ42." Such a peptide explores a much more restricted volume of conformational space than does its wild-type homologue, a volume comprising oligomeric conformational states of lower overall free energies or relatively high transitional activation energies. In the mirror-image experiment involving turn destabilization, the oligomer distribution of [*pP*]Aβ42 was indistinguishable, within experimental error, from that of Aβ40. This demonstrates that destabilization of the C terminal β-turn converts Aβ42 into Aβ40.

Unlike wild-type or [*VPV*]Aβ42, [*VPV*]Aβ40 formed β-rich fibrillar structures, though at slower pace than Aβ42 and Aβ40. This was not surprising considering the decreased number of hydrogen bond donors/acceptors and the decreased hydrophobic interaction potential at the C-terminus of the Aβ40 peptides compared with the Aβ42 peptides. Only three residues exist after the turn proper in the Aβ40 system, as opposed to five in the Aβ42 system. This means that although the VPV substitution enables formation of a relatively stable turn, the overall stability is lower due to the lack of the other two amino acids. Nevertheless, the VPV substitutions alone are sufficient to support β-turn formation at residues 36 and 37 of Aβ40 and thus produce a C-terminal structure engendering Aβ42-like behavior in [*VPV*]Aβ40.

Aβ42 formed assemblies resembling strings of spherical oligomers at t_β = 50% (Fig. 9), the midpoint

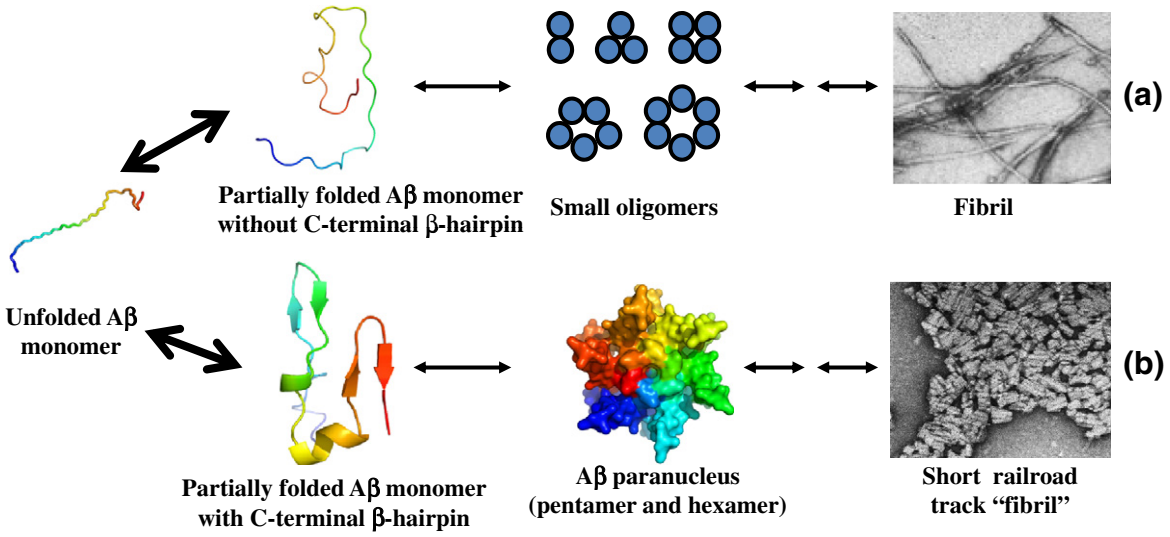

Fig. 13. A proposed mechanism for Aβ assembly. Aβ monomer can adopt two different types of conformation, one without and the other with a C-terminal β-hairpin. The former may form small oligomers that eventually deposit as amyloid fibrils, and the latter may form paranuclei and ultimately form "railroad-track-like fibrils." Big arrows indicate a rapid equilibrium among unfolded Aβ monomer and partially folded monomers. The Aβ monomeric structure is colored from blue (N-terminus) to red (C-terminus). Oligomers in each pathway may have different structures. The structure of the hexamer in the lower pathway is but one of a number of possible structures that were determined computationally.

of the assembly process. These structures also were observed with [*VPV*]Aβ42, but they remained dispersed and did not coalesce into protofibrils, suggesting that the [*VPV*]Aβ42 oligomers were more stable than those formed by Aβ42. Assemblies formed by both peptides exhibited significant and similar levels of neurotoxic activity (Fig. 12). After 5 days of incubation, Aβ42 formed amyloid fibrils and [*VPV*]Aβ42 formed quasicrystalline structures. Interestingly, at this time point, Aβ42 toxicity declined. This might have been due to the formation of macromolecular aggregates that had decreased intrinsic toxicity or decreased ability to diffuse to and interact with cell membranes. In contrast, the toxicity of [*VPV*]Aβ42, which remained in oligomeric form, remained undiminished. [*pP*]Aβ42 also was toxic and its toxicity remained high both at $t_{\beta}=50\%$ and at $t_{\beta}=100\%$. For each mutant Aβ42 peptide, substantially less higher-order assembly was observed relative to the wild-type peptide form, consistent with an enhanced toxic potency of the oligomeric assemblies.[16,17] Consistent with a potential relationship between oligomer content and toxicity, [*VPV*]Aβ40 was quite toxic in MTS and LDH assays, unlike its wild-type homologue. In addition, after incubation for 5 days, [*VPV*]Aβ40 toxicity was equivalent to that of wild-type Aβ42 (Fig. 12), as would be predicted for an Aβ42-like peptide.

In previous experiments, we produced pure, stable dimers, trimers, and tetramers of Aβ40 and showed that each species seeded growth of amyloid fibrils.[16] Seeding capacity depended directly on the extent of structural order within each oligomer population, as determined by CD and ThT analyses. This suggested that these oligomers shared at least some structural features with fibrils. Pentamers and hexamers were not studied. Fibril models have suggested that the C-termini of Aβ40 and Aβ42 form parallel, in-register β-strands.[40,41] However, structural diversity exists among fibril populations because differences in fibril preparation method produce fibrils of differing morphology.[42] Our results provide one mechanistic interpretation for these results, namely, that differences in monomer C-terminal structure drive assembly down different pathways (Fig. 13). In the simplest case, low-order oligomers (dimers, trimers, tetramers, and certain types of pentamer or hexamer) possess C-termini that do not form β-hairpins. This state exists not only in the Aβ40 system in particular[14] but also in the Aβ42 system, and it gives rise to classical amyloid-type fibrils (Fig. 13a). When stable C-terminal β-hairpins do exist, pentamers and hexamers (paranuclei) are stabilized, which simultaneously hinders the formation of dimers, trimers, and tetramers (Fig. 13b). One mechanism for this stabilization may be the increase in hydrophobic surface created by turn formation at residues 35–38, which facilitates inter- and intrapeptide interactions leading to and stabilizing oligomers. This is especially evident in the case of [*VPV*]Aβ42. The result of this stabilization is subsequent formation of distinct fibrillar structures with relatively small aspect ratios and a unique ("railroad tracks and ties") morphology.

In contrast, [*pP*]Aβ42 cannot form paranucleus because its C-terminus cannot fold into the

necessary β-hairpin structure. Other C-terminal turns may exist. Ahmed *et al.*, using low-temperature and low-salt conditions to produce Aβ42 pentamers, reported that residues 37 and 38 underwent hydrogen–deuterium exchange, whereas flanking residues did not, suggesting that these two residues adopted a turn-like conformation.[43] This turn position previously had been proposed in *in silico* modeling studies.[24,44] More recently, Rajadas *et al.* replaced Gly37–Gly38 with Pro–Gly and found that the substitutions caused Aβ42 to form more stable oligomers, but these oligomers were relatively disordered.[45] It is noteworthy that a recent study suggested that β-hairpins involving Gly–Gly are relatively unstable.[29] Murakami *et al.* suggested that a turn is centered at residues 38–39 and that this turn may be responsible for bringing the C-terminal carboxylate anion close to an *S*-oxidized radical cation of Met35, thus stabilizing it.[46] These other turn positions are different from that reported here but, taken together, emphasize the importance of C-terminal turn formation in controlling Aβ oligomerization and higher-order assembly.

Recently, a very interesting new structure, the "cylindrin," was described.[47] This hexamer of peptide undecamers forms a cylindrical structure that has secondary-structure, immunological ($A11^+$), and toxicity characteristics similar to those of Aβ paranuclei. It is possible that one or more short Aβ peptide segments could form a cylindrical core that organizes paranucleus formation. No evidence yet exists for this possibility, but the question currently is under active study.

In summary, our data suggest that the C-terminal Val36–Gly37 turn is the *sine qua non* of Aβ42. Facilitating its formation in Aβ40 creates a more Aβ42-like peptide. Stabilizing the turn in Aβ42 creates a "super Aβ42." The VPV substitutions stabilized the β-hairpin and facilitated Aβ42 paranuclei formation. [*VPV*]Aβ42 assemblies were neurotoxic and comprised a population with few classical amyloid-type fibrils but with substantial numbers of unusual, short, quasicrystalline structures resembling railroad tracks and ties. Destabilizing the turn in Aβ42 makes this peptide "Aβ40-like." This makes the turn a particularly attractive and important target for therapeutic agents. In addition, our engineered mutants should be useful tools for mechanistic studies of Aβ neurotoxicity because of the relatively high stability of the oligomers formed.

Materials and Methods

Molecular dynamics simulation

We previously used the Generalized Born implicit solvent model[48] and REMD for our simulations, obtaining a qualitative picture of the conformational dynamics of full-length Aβ40 and Aβ42.[23] However, modeling solvent implicitly may preclude the definition of the high-resolution structure of Aβ because these models do not represent the explicit atomic interactions between water and protein molecules and they may underestimate the frictional effects of water molecules surrounding the protein.[48] As a result, peptide populations may appear to possess higher conformational freedom and lower structural stability, when in fact they do not.

Simulation using full-length Aβ in explicit water remains impractical, as it requires enormous computational resources.[23] For this reason, we study the representative C-terminal folding units of Aβ40 and Aβ42, Aβ(31–40), and Aβ(31–42), respectively. Aβ[23] and many other proteins[49] comprise autonomous or semiautonomous folding units ("foldons").[50] The study of the conformational dynamics of these foldons can provide information relevant to the segmental folding of the holoprotein.[49,50] For Aβ, a large body of computational work has been done successfully on the Aβ(21–30) segment that comprises a peptide monomer folding nucleus.[27,51–54] These computational studies confirmed and extended prior experimental studies of the decapeptide and of the full-length Aβ peptide.[27,55]

Simulations were performed with the SANDER module of the Amber simulation package (version 10).[56] The peptides were modeled by PARM99SB, a recently improved all-atom force field.[57] An extended copy of the peptide was heated to 300 K and subjected to a 20-ps MD run. The final conformation was then used as the starting conformation for the production runs. The starting conformers were desolvated in an octahedral TIP3P water box.[58] The minimum distance of a protein atom to the edge of the box was 12 Å. A single Na^+ ion was added to the system to maintain system neutrality. This system models a very dilute aqueous peptide solution at neutral pH. The system was minimized by 1000 steps of energy minimization to release geometry collision before being subjected to 500 ps of equilibration at NTP (1 bar and 298 K). REMD simulations then were performed. Sixty-four replicas that exponentially spanned the temperature range 270–600 K were created. The temperature of the system was regulated using the Langevin dynamics algorithm[59] with a collision frequency of 3.0 ps^{-1}. The particle mesh Ewald summation method[60] was used to treat the long-range electrostatic interaction. During the simulation, hydrogen atoms were constrained using the SHAKE algorithm.[61] The integration time step was 2 fs. Exchange between replicas was attempted every 2 ps. Other relevant parameters were set by default. For each replica, the simulation length was 50 ns and 50,000 conformations were collected. The first 30 ns was treated as equilibration and the last 20 ns was used for data analysis.

In our studies here, each peptide was subjected to 50 ns of REMD simulations at 298 K. The first 30 ns was used to equilibrate the system. The production run comprised 20,000 conformations collected from the last 20 ns. To determine if the simulation had converged, we divided the last 20 ns of data into two equal parts and then subjected each to secondary-structure analysis using DSSP.[28] The extent of overlap of the curves suggests that the two conformational ensembles are highly similar, indicating convergence (Fig. S1).

Peptide synthesis

Aβ40, Aβ42, and their analogues were synthesized using 9-fluorenylmethoxycarbonyl chemistry and purified by reverse-phase high-performance liquid chromatography, essentially as previously described.[62] The identity and purity (usually >97%) of the peptides were confirmed by amino acid analysis followed by mass spectrometry and reverse-phase high-performance liquid chromatography.

Preparation of low-molecular-weight Aβ42

Two hundred micrograms of each peptide lyophilizate was dissolved in 10% (v/v) 60 mM NaOH, followed by 45% (v/v) MilliQ water. The pH was adjusted to 7.5 by addition of 45% (v/v) 10 mM sodium phosphate, pH 7.5, yielding final nominal concentrations of 25–80 μM (depending on the experiment) in 4.5 mM phosphate buffer, pH 7.5. The peptide solution was then sonicated for 1 min in a Branson ultrasonic water bath (Branson Ultrasonics Corp., Danbury CT) and then centrifuged at 16,000***g*** at room temperature (RT; usually 22 °C) for 10 min. The supernatant fluid was filtered using a 0.2-μm Anotop filter and placed on ice. The filtrate is defined as "low-molecular-weight" (LMW) Aβ and comprises an equilibrium mixture of monomer and low-order oligomers.[63] Protein concentrations of these and other preparations were determined by quantitative amino acid analysis, unless otherwise indicated.

Photo-induced chemical cross-linking of Aβ

Aβ oligomerization was studied using PICUP,[18] essentially as previously described.[64] Briefly, LMW Aβ was prepared at a concentration of 25–35 μM in 4.5 mM sodium phosphate, pH 7.5, at RT. Cross-linking was performed by adding 18 μL of sample to a 0.2-ml volume PCR tube. One microliter of 2 mM Tris (2,2′-bipyridyl) dichlororuthenium (II)hexahydrate [Ru (bpy)] and 1 μL of 40 mM ammonium persulfate were then added, after which the tube was irradiated for 1 s with visible light. The reaction was quenched immediately with 1 μL of 1 M dithiothreitol and the sample was then placed on ice. An equal volume of 2× Tris–*N*-[2-hydroxy-1,1-bis(hydroxymethyl)ethyl]glycine SDS sample buffer was added to each sample. The samples were boiled in a 100 °C water bath for 10 min, centrifuged for 5–10 s at 16,000***g***, and then electrophoresed on a 10–20% T 1-mm-thick Tris–*N*-[2-hydroxy-1,1-bis(hydroxymethyl)ethyl]glycine SDS gel. The gel was silver stained using an Invitrogen X-press silver staining kit.

Circular dichroism spectroscopy

LMW Aβ solutions were prepared at a concentration of 60–80 μM. After sonication, the peptide samples were incubated at 37 °C with slow inversion on a MiniLabroller (Edison, NJ). CD spectroscopy was then performed every 24 h using a JASCO J-810 spectropolarimeter (Tokyo, Japan). The CD parameters were as follows: wavelength range of 190–260 nm, data pitch of 0.2 nm, continuous scan mode, scan speed of 100 nm/min, 1 s response, bandwidth of 2 nm, and an accumulation of 10 scans per sample. The spectra were smoothed using the different adaptive smoothing parameters within the data acquisition software (Spectra Manager). The data subsequently were deconvoluted using DichroWeb.[32]

ThT fluorescence

ThT is a fluorescent dye that has been used to measure the time-dependent acquisition of β-sheet structure associated with fibrillar assemblies. ThT fluorescence does not measure fibril concentration *per se* (some fibrils do not possess the β-sheet structures to which ThT binds), but fluorescence intensities do correlate with Aβ fibril content.[33] LMW Aβ peptides were prepared at nominal concentrations of 35–40 μM. The samples were incubated with slow end-over-end mixing (inversion) on a MiniLabroller. At 24-h intervals, 10 μL of each sample was removed and added to 190 μL of 20 μM ThT dissolved in the same buffer. The solution was vortexed gently and incubated for 5 min at RT, and then fluorescence was determined using a Hitachi 4500 fluorimeter (Tokyo, Japan). Readings were obtained at an excitation wavelength of 450 nm and an emission wavelength of 482 nm. The slit widths were 5 nm and 10 nm, respectively. The readings were repeated three times at intervals of 30 s and the mean of the blank-corrected three readings was calculated. "Blanks" contained 20 μM ThT in buffer.

Dynamic light scattering spectroscopy

DLS complements PICUP.[36] It requires no chemical stabilization of oligomers and its sensitivity increases with increasing oligomer molecular weight. PICUP, in contradistinction, is particularly useful for quantitation of low-order oligomer frequency distributions, but because cross-linking efficiency is <100%, it becomes increasingly inaccurate as molecular weight rises. Figure S1 shows the temporal evolution of the size distributions of the wild-type and modified Aβ peptides. Aβ40, Aβ42, and their respective mutants were dissolved at a concentration of 0.5 mg/ml in 20 mM sodium phosphate buffer, pH 7.5, briefly vortexed, sonicated for 20 s, and filtered using a 20-nm Anotop filter. Samples were subjected to DLS spectroscopy at RT for 7–10 days. Measurements were done using a custom optical setup comprising a 40-mW He–Ne laser (λ = 633 nm) (Coherent, Santa Clara, CA) and a PD2000DLS detector/correlator unit (Precision Detectors, Bellingham, MA). Light scattering was measured at an angle of 90°. The intensity correlation function and the diffusion constant (D) frequency distribution were determined using Precision Deconvolve software (Precision Detectors). Hydrodynamic radius (R_H) values were obtained from those for D using the Stokes–Einstein relationship,[11] $D = k_B T/6\pi\eta R_H$, allowing inferences to be made about the distribution of scatterer sizes.

Electron microscopy

Formvar 400-mesh grids were glow discharged on a MED 010 EM glow discharge apparatus containing a

cylindrical discharge compartment and an adjacent discharge control and timer unit. Peptide samples were mixed thoroughly and 8 μL of sample was layered carefully on the grid. The grid was incubated for 20 min under cover to prevent dust accumulation. After incubation, the solution was carefully drained using a filter paper wick by gently touching the tip of the filter paper to the edge of the grid. Five microliters of 2.5% (v/v) glutaraldehyde was added to the grid, which was then incubated for 3 min in the absence of light. The glutaraldehyde solution was removed after incubation using a filter paper wick. Five microliters of 1% (w/v) uranyl acetate was applied to the grid, which was incubated for 3 min in the dark. The solution was blotted away and the grids were air dried and examined on a JEOL 1200 EX transmission electron microscope.

Primary neuronal cultures

Rat cortical cultures were established from embryonic day 17 fetuses, as described previously.[65] Briefly, the brain tissue was dissociated into a single-cell suspension by incubation with 0.25% trypsin/phosphate-buffered saline at 37 °C for 30 min and mechanical dissociation using a fire-polished glass Pasteur pipette. Cells were plated at a density of 20,000 cells/cm^2 on glass coverslips in 35- and 100-mm culture dishes. Two hours after plating, the medium was changed to Neurobasal plus N2 and B27 supplements (Invitrogen, Grand Island, NY). Cells were maintained at 37 °C and 5% CO_2 with 50% of the medium changed every 5 days. Cells were treated with various preparations of Aβ at 14 days *in vitro* for 12 and 24 h.

Neurotoxicity assays

Cell death was assessed by quantifying LDH release using the CytoTox 96 kit (Promega, Madison, WI).[66] Cells were treated with Aβ peptides removed at different time points from the CD reaction mixtures. Each aliquot was snap frozen in liquid nitrogen and then stored at −85 °C until assay. LDH released into the culture supernate due to Aβ-induced cell lysis was measured with a 30-min coupled enzymatic assay that resulted in the conversion of a tetrazolium salt (INT) into a red formazan product. The amount of color formed is proportional to the number of lysed cells.

Mitochondrial oxidoreductase activity was determined by analyzing the conversion of a tetrazolium compound to formazan. The reagent MTS is reduced to formazan by mitochondrial succinate dehydrogenase in complex II (succinate/ubiquinone oxidoreductase complex) and possibly other complexes of the electron transport chain (CellTiter 96 AQueous; Promega).[66] The quantity of formazan product measured by A_{490} is directly proportional to the number of living cells in culture.

Protein concentrations were determined using the BCA protein assay kit (Thermo Scientific, CA), using the microtiter plate protocol. The concentrations of the Aβ40 and Aβ42 peptides were adjusted with 10 mM sodium phosphate, pH 7.5, to maintain uniformity. The final peptide concentration used in both assays was 2.5 μM.

Acknowledgements

We thank Margaret Condron for synthesizing all the peptides used here. We gratefully acknowledge grants from the State of California Alzheimer's Disease Research Fund (No. 07-65806), UCLA Faculty Research Fund, the National Institutes of Health (AG027818, NS038328), and the Jim Easton Consortium for Alzheimer's Drug Discovery and Biomarkers.

Supplementary Data

Supplementary data to this article can be found online at http://dx.doi.org/10.1016/j.jmb.2012.11.006

Received 30 July 2012;
Received in revised form 25 October 2012;
Accepted 3 November 2012
Available online 12 November 2012

Keywords:
amyloid β-protein;
Alzheimer's disease;
β-hairpin

† R.R. and M.Y. are co-first authors.

‡ Throughout this publication, we refer to both the "turn" and the "hairpin." The former term is restricted to Val36 and Gly37 and its neighboring residues, Met35 and Gly38, which are involved in H-bond formation that stabilizes the turn. The term "hairpin" refers to the global structure of the Aβ(31–42) peptide, a structure that must possess a turn to exist.

§ In the context of oligomerization experiments, the term "order" refers to the number of Aβ monomers comprising the assembly.

Abbreviations used:
AD, Alzheimer's disease; Aβ, amyloid β-protein; DLS, dynamic light scattering; EM, electron microscopy; LDH, lactate dehydrogenase; LMW, low molecular weight; MTS, 3-[4,5-dimethylthiazol-2-yl]-5-[3-carboxymethoxyphenyl]-2-[4-sulfophenyl]-2*H*-tetrazolium; PICUP, photo-induced cross-linking of unmodified proteins; REMD, replica-exchange molecular dynamics; RT, room temperature; SC, statistical coil; ThT, thioflavin T.

References

1. Selkoe, D. J. (2001). Alzheimer's disease: genes, proteins, and therapy. *Physiol. Rev.* **81**, 741–766.
2. Selkoe, D. J. (1991). The molecular pathology of Alzheimer's disease. *Neuron*, **6**, 487–498.
3. Roychaudhuri, R., Yang, M., Hoshi, M. M. & Teplow, D. B. (2009). Amyloid β-protein assembly and Alzheimer disease. *J. Biol. Chem.* **284**, 4749–4753, http://dx.doi.org/10.1074/jbc.R800036200.

4. Glenner, G. G. & Wong, C. W. (1984). Alzheimer's disease: initial report of the purification and characterization of a novel cerebrovascular amyloid protein. *Biochem. Biophys. Res. Commun.* **120**, 885–890.
5. Gravina, S. A., Ho, L., Eckman, C. B., Long, K. E., Otvos, L., Younkin, L. H. *et al.* (1995). Amyloid β-protein (Aβ) in Alzheimer's disease brain. Biochemical and immunocytochemical analysis with antibodies specific for forms ending at Aβ40 or Aβ42(43). *J. Biol. Chem.* **270**, 7013–7016.
6. Iwatsubo, T., Odaka, A., Suzuki, N., Mizusawa, H., Nukina, N. & Ihara, Y. (1994). Visualization of Aβ 42(43) and Aβ40 in senile plaques with end-specific Aβ monoclonals: evidence that an initially deposited species is Aβ42(43). *Neuron*, **13**, 45–53.
7. Suzuki, N., Cheung, T. T., Cai, X. D., Odaka, A., Otvos, L., Eckman, C. *et al.* (1994). An increased percentage of long amyloid β-protein secreted by familial amyloid β-protein precursor (β APP717) mutants. *Science*, **264**, 1336–1340.
8. Golde, T. E., Eckman, C. B. & Younkin, S. G. (2000). Biochemical detection of Aβ isoforms: implications for pathogenesis, diagnosis, and treatment of Alzheimer's disease. *Biochim. Biophys. Acta*, **1502**, 172–187.
9. Scheuner, D., Eckman, C., Jensen, M., Song, X., Citron, M., Suzuki, N. *et al.* (1996). Secreted amyloid β-protein similar to that in the senile plaques of Alzheimer's disease is increased in vivo by the presenilin 1 and 2 and APP mutations linked to familial Alzheimer's disease. *Nat. Med.* **2**, 864–870.
10. Weggen, S., Eriksen, J. L., Das, P., Sagi, S. A., Wang, R., Pietrzik, C. U. *et al.* (2001). A subset of NSAIDs lower amyloidogenic Aβ42 independently of cyclooxygenase activity. *Nature*, **414**, 212–216, http://dx.doi.org/10.1038/35102591.
11. Lomakin, A., Teplow, D. B. & Benedek, G. B. (2005). Quasielastic light scattering for protein assembly studies. *Methods Mol. Biol.* **299**, 153–174.
12. Jarrett, J. T., Berger, E. P. & Lansbury, P. T. (1993). The carboxy terminus of the β-amyloid protein is critical for the seeding of amyloid formation: implications for the pathogenesis of Alzheimer's disease. *Biochemistry*, **32**, 4693–4697.
13. Lomakin, A., Chung, D. S., Benedek, G. B., Kirschner, D. A. & Teplow, D. B. (1996). On the nucleation and growth of amyloid β-protein fibrils: detection of nuclei and quantitation of rate constants. *Proc. Natl Acad. Sci. USA*, **93**, 1125–1129.
14. Bernstein, S. L., Dupuis, N. F., Lazo, N. D., Wyttenbach, T., Condron, M. M., Bitan, G. *et al.* (2009). Amyloid-β protein oligomerization and the importance of tetramers and dodecamers in the aetiology of Alzheimer's disease. *Nat. Chem.* **1**, 326–331, http://dx.doi.org/10.1038/nchem.247.
15. Bitan, G., Vollers, S. S. & Teplow, D. B. (2003). Elucidation of primary structure elements controlling early amyloid β-protein oligomerization. *J. Biol. Chem.* **278**, 34882–34889, http://dx.doi.org/10.1074/jbc.M300825200.
16. Ono, K., Condron, M. M. & Teplow, D. B. (2009). Structure–neurotoxicity relationships of amyloid β-protein oligomers. *Proc. Natl Acad. Sci. USA*, **106**, 14745–14750, http://dx.doi.org/10.1073/pnas.0905127106.
17. Dahlgren, K. N., Manelli, A. M., Stine, W. B., Baker, L. K., Krafft, G. A. & LaDu, M. J. (2002). Oligomeric and fibrillar species of amyloid-β peptides differentially affect neuronal viability. *J. Biol. Chem.* **277**, 32046–32053, http://dx.doi.org/10.1074/jbc.M201750200.
18. Fancy, D. A. & Kodadek, T. (1999). Chemistry for the analysis of protein–protein interactions: rapid and efficient cross-linking triggered by long wavelength light. *Proc. Natl Acad. Sci. USA*, **96**, 6020–6024.
19. Bitan, G., Kirkitadze, M. D., Lomakin, A., Vollers, S. S., Benedek, G. B. & Teplow, D. B. (2003). Amyloid β-protein (Aβ) assembly: Aβ40 and Aβ42 oligomerize through distinct pathways. *Proc. Natl Acad. Sci. USA*, **100**, 330–335, http://dx.doi.org/10.1073/pnas.222681699.
20. Lambert, M. P., Barlow, A. K., Chromy, B. A., Edwards, C., Freed, R., Liosatos, M. *et al.* (1998). Diffusible, nonfibrillar ligands derived from A31–42 are potent central nervous system neurotoxins. *Proc. Natl Acad. Sci. USA*, **95**, 6448–6453.
21. Lesné, S., Koh, M. T., Kotilinek, L., Kayed, R., Glabe, C. G., Yang, A. *et al.* (2006). A specific amyloid-β protein assembly in the brain impairs memory. *Nature*, **440**, 352–357, http://dx.doi.org/10.1038/nature04533.
22. Westlind-Danielsson, A. & Arnerup, G. (2001). Spontaneous in vitro formation of supramolecular β-amyloid structures, "βamy balls", by β-amyloid 1–40 peptide. *Biochemistry*, **40**, 14736–14743.
23. Yang, M. & Teplow, D. B. (2008). Amyloid β-protein monomer folding: free-energy surfaces reveal alloform-specific differences. *J. Mol. Biol.* **384**, 450–464, http://dx.doi.org/10.1016/j.jmb.2008.09.039.
24. Urbanc, B., Cruz, L., Yun, S., Buldyrev, S. V., Bitan, G., Teplow, D. B. & Stanley, H. E. (2004). In silico study of amyloid β-protein folding and oligomerization. *Proc. Natl Acad. Sci. USA*, **101**, 17345–17350, http://dx.doi.org/10.1073/pnas.0408153101.
25. Sgourakis, N. G., Yan, Y., McCallum, S. A., Wang, C. & Garcia, A. E. (2007). The Alzheimer's peptides Aβ40 and 42 adopt distinct conformations in water: a combined MD/NMR study. *J. Mol. Biol.* **368**, 1448–1457, http://dx.doi.org/10.1016/j.jmb.2007.02.093.
26. Hou, L., Shao, H., Zhang, Y., Li, H., Menon, N. K., Neuhaus, E. B. *et al.* (2004). Solution NMR studies of the Aβ(1–40) and Aβ(1–42) peptides establish that the Met35 oxidation state affects the mechanism of amyloid formation. *J. Am. Chem. Soc.* **126**, 1992–2005, http://dx.doi.org/10.1021/ja036813f.
27. Yan, Y. & Wang, C. (2006). Aβ42 is more rigid than Aβ40 at the C terminus: implications for Aβ aggregation and toxicity. *J. Mol. Biol.* **364**, 853–862, http://dx.doi.org/10.1016/j.jmb.2006.09.046.
28. Lazo, N. D., Grant, M. A., Condron, M. C., Rigby, A. C. & Teplow, D. B. (2005). On the nucleation of amyloid β-protein monomer folding. *Protein Sci.* **14**, 1581–1596, http://dx.doi.org/10.1110/ps.041292205.
29. Kabsch, W. & Sander, C. (1983). Dictionary of protein secondary structure: pattern recognition of hydrogen-bonded and geometrical features. *Biopolymers*, **22**, 2577–2637, http://dx.doi.org/10.1002/bip.360221211.
30. Gibbs, A. C., Bjorndahl, T. C., Hodges, R. S. & Wishart, D. S. (2002). Probing the structural determinants of type II′ β-turn formation in peptides and proteins. *J. Am. Chem. Soc.* **124**, 1203–1213.

31. Budesinsky, M., Sebestik, J., Bednarova, L., Baumruk, V., Safarik, M. & Bour, P. (2008). Conformational properties of the Pro-Gly motif in the D-Ala–L-Pro-Gly–D-Ala model peptide explored by a statistical analysis of the NMR, Raman, and Raman optical activity spectra. *J. Org. Chem.* **73**, 1481–1489, http://dx.doi.org/10.1021/jo702297y.
32. Rao, M. H. V. R., Kumar, S. K. & Kunwar, A. C. (2003). Formation of β-hairpins in L-Pro-Gly containing peptides facilitated by β-amino benzoic acid. *Tetrahedron Lett.* **44**, 7369–7372.
33. Whitmore, L. & Wallace, B. A. (2004). Dichroweb, an online server for protein secondary structure analyses from circular dichroism spectroscopic data. *Nucleic Acids Res.* **32**, W668–W673, http://dx.doi.org/10.1093/nar/gkh371.
34. Groenning, M. (2009). Binding mode of Thioflavin T and other molecular probes in the context of amyloid fibrils—current status. *J. Chem. Biol.* **3**, 1–18, http://dx.doi.org/10.1007/s12154-009-0027-5.
35. Qiang, W., Yau, W.-M. & Tycko, R. (2011). Structural evolution of Iowa mutant β-amyloid fibrils from polymorphic to homogeneous states under repeated seeded growth. *J. Am. Chem. Soc.* **133**, 4018–4029, http://dx.doi.org/10.1021/ja109679q.
36. Bitan, G. & Teplow, D. B. (2004). Rapid photochemical cross-linking—a new tool for studies of metastable, amyloidogenic protein assemblies. *Acc. Chem. Res.* **37**, 357–364, http://dx.doi.org/10.1021/ar000214l.
37. Lomakin, A. & Teplow, D. B. (2006). Quasielastic light scattering study of amyloid β-protein fibril formation. *Protein Pept. Lett.* **13**, 247–254.
38. Lobner, D. (2000). Comparison of the LDH and MTT assays for quantifying cell death: validity for neuronal apoptosis? *J. Neurosci. Methods*, **96**, 147–152.
39. Cerf, E., Sarroukh, R., Tamamizu-Kato, S., Breydo, L., Derclaye, S., Dufr64ne, Y. *et al.* (2009). Anti-parallel β-sheet—a signature structure of the oligomeric amyloid-β peptide. *Biochem. J.* **421**, 415–423, http://dx.doi.org/10.1042/BJ20090379.
40. Petkova, A. T., Ishii, Y., Balbach, J. J., Antzutkin, O. N., Leapman, R. D., Delaglio, F. & Tycko, R. (2002). A structural model for Alzheimer's β-amyloid fibrils based on experimental constraints from solid state NMR. *Proc. Natl Acad. Sci. USA*, **99**, 16742–16747, http://dx.doi.org/10.1073/pnas.262663499.
41. Lührs, T., Ritter, C., Adrian, M., Riek-Loher, D., Bohrmann, B., Dobeli, H. *et al.* (2005). 3D structure of Alzheimer's amyloid-β(1–42) fibrils. *Proc. Natl. Acad. Sci. USA*, **102**, 17342–17347.
42. Petkova, A. T., Leapman, R. D., Guo, Z., Yau, W.-M., Mattson, M. P. & Tycko, R. (2005). Self-propagating, molecular-level polymorphism in Alzheimer's β-amyloid fibrils. *Science*, **307**, 262–265, http://dx.doi.org/10.1126/science.1105850.
43. Ahmed, M., Davis, J., Aucoin, D., Sato, T., Ahuja, S., Aimoto, S. *et al.* (2010). Structural conversion of neurotoxic amyloid-β(1–42) oligomers to fibrils. *Nat. Struct. Mol. Biol.* **17**, 561–567, http://dx.doi.org/10.1038/nsmb.1799.
44. Kelley, N. W., Vishal, V., Krafft, G. A. & Pande, V. S. (2008). Simulating oligomerization at experimental concentrations and long timescales: a Markov state model approach. *J. Chem. Phys.* **129**, 214707, http://dx.doi.org/10.1063/1.3010881.
45. Rajadas, J., Liu, C. W., Novick, P., Kelley, N. W., Inayathullah, M., Lemieux, M. C. & Pande, V. S. (2011). Rationally designed turn promoting mutation in the amyloid-β peptide sequence stabilizes oligomers in solution. *PLoS One*, **6**, e21776, http://dx.doi.org/10.1371/journal.pone.0021776.
46. Murakami, K., Irie, K., Ohigashi, H., Hara, H., Nagao, M., Shimizu, T. & Shirasawa, T. (2005). Formation and stabilization model of the 42-mer Aβ radical: implications for the long-lasting oxidative stress in Alzheimer's disease. *J. Am. Chem. Soc.* **127**, 15168–15174, http://dx.doi.org/10.1021/ja054041c.
47. Laganowsky, A., Liu, C., Sawaya, M. R., Whitelegge, J. P., Park, J., Zhao, M. *et al.* (2012). Atomic view of a toxic amyloid small oligomer. *Science*, **335**, 1228–1231, http://dx.doi.org/10.1126/science.1213151.
48. Bashford, D. & Case, D. A. (2000). Generalized Born models of macromolecular solvation effects. *Annu. Rev. Phys. Chem.* **51**, 129–152, http://dx.doi.org/10.1146/annurev.physchem.51.1.129.
49. Maity, H., Maity, M., Krishna, M. M. G., Mayne, L. & Englander, S. W. (2005). Protein folding: the stepwise assembly of foldon units. *Proc. Natl Acad. Sci. USA*, **102**, 4741–4746, http://dx.doi.org/10.1073/pnas.0501043102.
50. Panchenko, A. R., Luthey-Schulten, Z. & Wolynes, P. G. (1996). Foldons, protein structural modules, and exons. *Proc. Natl Acad. Sci. USA*, **93**, 2008–2013.
51. Cruz, L., Urbanc, B., Borreguero, J. M., Lazo, N. D., Teplow, D. B. & Stanley, H. E. (2005). Solvent and mutation effects on the nucleation of amyloid β-protein folding. *Proc. Natl Acad. Sci. USA*, **102**, 18258–18263, http://dx.doi.org/10.1073/pnas.0509276102.
52. Baumketner, A., Bernstein, S. L., Wyttenbach, T., Lazo, N. D., Teplow, D. B., Bowers, M. T. & Shea, J.-E. (2006). Structure of the 21–30 fragment of amyloid β-protein. *Protein Sci.* **15**, 1239–1247, http://dx.doi.org/10.1110/ps.062076806.
53. Chen, W., Mousseau, N. & Derreumaux, P. (2006). The conformations of the amyloid-β (21–30) fragment can be described by three families in solution. *J. Chem. Phys.* **125**, 084911, http://dx.doi.org/10.1063/1.2337628.
54. Fawzi, N. L., Phillips, A., Ruscio, J., Doucleff, M., Wemmer, D. & Head-Gordon, T. (2008). Structure and dynamics of the Aβ21–30 peptide from the interplay of NMR experiments and molecular simulations. *J. Am. Chem. Soc.* **130**, 6145–6158, http://dx.doi.org/10.1021/ja710366c.
55. Grant, M. A., Lazo, N. D., Lomakin, A., Condron, M. M., Arai, H., Yamin, G. *et al.* (2007). Familial Alzheimer's disease mutations alter the stability of the amyloid β-protein monomer folding nucleus. *Proc. Natl Acad. Sci. USA*, **104**, 16522–16527, http://dx.doi.org/10.1073/pnas.0705197104.
56. Case, D., Darden, T., Cheatham, T., Wang, C. S. III, J., Duke, R., Luo, R. *et al.* (2004). Amber 8, University of California, San Francisco.
57. Hornak, V., Abel, R., Okur, A., Strockbine, B., Roitberg, A. & Simmerling, C. (2006). Comparison of multiple Amber force fields and development of improved protein backbone parameters. *Proteins*, **65**, 712–725, http://dx.doi.org/10.1002/prot.21123.

58. Jorgensen, W. L., Chandrasekhar, J., Madura, J. D., Impey, R. W. & Klein, M. L. (1983). Comparison of simple potential functions for simulating liquid water. *J. Chem. Phys.* **79**, 926–935.
59. Lamm, G. & Szabo, A. (1986). Langevin modes of macromolecules. *J. Chem. Phys.* **85**, 7334–7348.
60. Darden, T., York, D. & Pedersen, L. (1993). Particle mesh Ewald: a *N*-log(*n*) method for Ewald sums in large systems. *J. Chem. Phys.* **98**, 10089–10092.
61. Ryckaert, J.-P., Ciccotti, G. & Berendsen, H. J. C. (1977). Numerical integration of the cartesian equations of motion of a system with constraints: molecular dynamics of n-alkanes. *J. Comput. Phys.* **23**, 327–341.
62. Walsh, D. M., Lomakin, A., Benedek, G. B., Condron, M. M. & Teplow, D. B. (1997). Amyloid β-protein fibrillogenesis. Detection of a protofibrillar intermediate. *J. Biol. Chem.* **272**, 22364–22372.
63. Walsh, D. M., Hartley, D. M., Kusumoto, Y., Fezoui, Y., Condron, M. M., Lomakin, A. *et al.* (1999). Amyloid β-protein fibrillogenesis. Structure and biological activity of protofibrillar intermediates. *J. Biol. Chem.* **274**, 25945–25952.
64. Bitan, G., Lomakin, A. & Teplow, D. B. (2001). Amyloid β-protein oligomerization: prenucleation interactions revealed by photo-induced cross-linking of unmodified proteins. *J. Biol. Chem.* **276**, 35176–35184, http://dx.doi.org/10.1074/jbc.M102223200.
65. Ma, Q.-L., Yang, F., Calon, F., Ubeda, O. J., Hansen, J. E., Weisbart, R. H. *et al.* (2008). p21-activated kinase-aberrant activation and translocation in alzheimer disease pathogenesis. *J. Biol. Chem.* **283**, 14132–14143, http://dx.doi.org/10.1074/jbc.M708034200.
66. Deshpande, A., Mina, E., Glabe, C. & Busciglio, J. (2006). Different conformations of amyloid-β induce neurotoxicity by distinct mechanisms in human cortical neurons. *J. Neurosci.* **26**, 6011–6018, http://dx.doi.org/10.1523/JNEUROSCI.1189-06.2006.